



AMERICAN UNIVERSITY OF BEIRUT

DISPLACEMENT VENTILATION WITH COOLED LIQUID  
DESICCANT DEHUMIDIFIER MEMBRANE AT CEILING;  
MODELING AND DESIGN CHARTS

by  
MOHAMAD BADIH HOUT

A thesis  
submitted in partial fulfillment of the requirements  
for the degree of Master of Mechanical Engineering  
to the Department of Mechanical Engineering  
of the Faculty of Engineering and Architecture  
at the American University of Beirut

Beirut, Lebanon  
August 2017

AMERICAN UNIVERSITY OF BEIRUT

DISPLACEMENT VENTILATION WITH COOLED LIQUID  
DESICCANT DEHUMIDIFIER MEMBRANE AT CEILING;  
MODELING AND DESIGN CHARTS

by  
MOHAMAD BADIH HOUT

Approved by:


Prof. Kamel Abou Ghali, PhD, Professor  
Department of Mechanical Engineering

  
Co-Advisor


Prof. Nesreen Ghaddar, PhD, Professor  
Department of Mechanical Engineering

  
Co-Advisor

Prof. Fadl Moukalled, PhD, Professor  
Department of Mechanical Engineering

  
Member of Committee

Prof. Ghanem Oweis, PhD, Associate Professor  
Department of Mechanical Engineering

  
Member of Committee

Date of thesis defense: August 30, 2017



## ACKNOWLEDGMENTS

First and foremost, I would like to show my sincere gratitude towards my advisors, Professor Kamel Abou Ghali and Professor Nesreen Ghaddar for constantly providing me with their never-ending knowledge and support during my Master's here at the American University of Beirut. Without their council, none of this work would have been possible.

I would also like to give a huge thanks to Dr. Nagham Ismail Younis for providing me with her valuable experience and guiding me through this project whenever things got tough. Special thanks goes to my colleagues and future Drs Mariam Itani and Douaa Al-Assaad for always supporting me whenever I needed help and motivation.

I would also like to express my gratitude towards all my colleagues here at AUB, special thanks goes to Hussein Daoud, Manar Younis, Walid Abou Hweij, Omar Hatoum, Omar El Hajj, Mohammad Kazzaz, Dr. Carine Habchi, Abed I Kader Saidi, Mohammad Allouche, Mohammad Sleiman, Mohammad Ghadban, Abd El Kader Ba'ayoun, Racha Seblany, Zeinab Ghaddar, Jinane Charara.

Special thanks goes to the FYP group for their help in manufacturing the experimental setup and running the experiments.

Last but not least, huge thanks goes to all the staff here in the Mechanical department, especially, Hisham, Dory, Roger, Ghassan and Joseph.

Finally, I would like to show sincere and deep gratitude towards my dear family: my father, my mother and my sister and my aunts, thank you for being there for me whenever I needed your emotional support.

# AN ABSTRACT OF THE THESIS OF

Mohamad Badih Hout

for Master of Engineering  
Major: Mechanical Engineering

Title: Displacement Ventilation with Cooled Liquid Desiccant Dehumidifier Membrane at Ceiling; Modeling and Design Charts.

A novel transport model is developed for a space conditioned by a cooled liquid desiccant dehumidification membrane ceiling (LDMC-C) and displacement ventilation DV in which the space is divided into three zones: an occupied cool with fresh air zone; an upper recirculation zone; and a ceiling adjacent boundary layer zone where the air is drawn at the exhaust grill. The adjacent air boundary layer at the ceiling membrane predicted the latent and sensible heat transfer to the desiccant solution. The boundary model was validated experimentally in a climatic chamber.

The developed model predicted of the LDMC-C/DV system operational parameters such as the supply flow rate and temperature and the liquid desiccant concentration, flow rate, and inlet temperature that meet thermal comfort and air quality requirements. Extensive simulations were performed on a typical office load of 75 W/m<sup>2</sup> to generate design charts of the system for three DV supply air temperatures of 18, 20, and 22 °C to identify the appropriate DV flow rate and inlet desiccant (CaCl<sub>2</sub>) solution temperature that provides comfort and air quality and ensures that condensation is unlikely to occur. The LDMC sensible and latent load removal from the space load is directly read off the charts.

# CONTENTS

ACKNOWLEDGMENTS.....	v
ABSTRACT.....	vi
LIST OF NOMENCLATURE.....	ix
LIST OF ILUSTRATIONS.....	xii
LIST OF TABLES .....	xiv
Chapter	
I. COOLED LIQUID DESICCANT DEHUMIDIFICATION MEMBRANE CEILING & DISPLACEMENT VENTILATION.....	1
A. Introduction: .....	1
B. System Description:.....	5
II. DEVELOPMENT & INTEGRATION OF BL-DEHUMIDIFIER MODEL WITH SPACE MODEL SYSTEM.....	7
A. Mathematical model of ceiling dehumidifier (air layer and liquid desiccant flow sides) ...	8
B. Liquid desiccant flow side.....	9
C. Air boundary layer side .....	10
D. Integration with space model system.....	13
E. Numerical Methodology.....	15
III. EXPERIMENTAL SETUP & MODEL VALIDATION .....	18
A. The membrane ceiling panel .....	18
B. The experimental setup.....	19
C. Experimental measurements and protocol.....	20
D. Experimental Validation of the mathematical model .....	23
IV. GENERATION OF DESIGN CHARTS FOR THE APPROPRIATE OPERATIONAL CONDITIONS OF LDMC-C/DV SYSTEM.....	26
V. CASE STUDY.....	30

A. Description of the LDMC-C/DV design charts with an example.....	32
B. Conclusion.....	36
<b>BIBLIOGRAPHY</b> .....	37
<b>APPENDIX</b> .....	43



## NOMENCLATURE

$A$	area ( m <sup>2</sup> )
$C$	concentration of water per desiccant (kg of H <sub>2</sub> O/kg CaCl <sub>2</sub> )
$CC$	chilled ceiling
$C_{in}$	Inlet concentration of the liquid desiccant
$C_p$	specific heat (J/kg·K)
$D$	diffusion constant of vapor in the pipe wall material (m <sup>2</sup> /s)
$DV$	displacement ventilation
$H_s$	stratification height (m)
$h_{ci}$	heat convection coefficient inside the dehumidifier (W/m <sup>2</sup> ·s)
$h_{co}$	heat convection coefficient outside the dehumidifier (W/m <sup>2</sup> ·s)
$h_{mo}$	mass convection coefficient outside the dehumidifier (m/s)
$h_{fg}$	latent heat of vaporization of the water (J/kg)
$h_d$	enthalpy of the liquid desiccant solution (J/kg)
$h_s$	enthalpy of supply air(J/kg)
$k$	thermal conductivity (W/m·K)
$L_p$	length of the dehumidifier panel (m)
$LDMC-C/DV$	liquid desiccant membrane cycle at the ceiling combined with displacement ventilation (DV) system
$\dot{m}$	mass flow rate (kg/s)
$Q$	upward volumetric flow rate (m <sup>3</sup> /s)

$q$	rate of heat transfer (W)
$Re_y$	local Reynolds number
$t$	membrane thickness (m)
$T$	temperature (°C)
$T_a$	indoor room (°C)
$T_\infty$	ambient temperature (°C)
$T_w$	wall temperature (°C)
$T_{sol}$	Liquid desiccant solution temperature (°C)
$T_s$	supply air temperature (°C)
$T_{in}$	Inlet temperature of the liquid desiccant(°C)
$U$	overall heat conductance coefficient of permeable pipe per unit length
$U_m$	overall mass conductance coefficient of permeable pipe per unit length
$V$	velocity of supply air (m/s)
$W_m$	width of the membrane (m)
$w$	humidity ratio (kg of H <sub>2</sub> O/kg of dry air)
$x$	horizontal distance from the inlet of the membrane (m)

### **Greek Letters**

$\omega_{sol}^*$	the solution equilibrium humidity ratio (kg <sub>H<sub>2</sub>O</sub> /kg <sub>dry air</sub> )
$\omega_a$	indoor room humidity ratio (kg <sub>H<sub>2</sub>O</sub> /kg <sub>dry air</sub> )
$\delta$	boundary layer thickness (m)
$\mu$	dynamic viscosity (kg/m <sup>2</sup> .s)
$\rho$	density (kg/m <sup>3</sup> )

## Subscripts

<i>a</i>	room air
<i>BL</i>	boundary layer
<i>c</i>	heat convection
<i>d</i>	CaCl <sub>2</sub> and H <sub>2</sub> O desiccant solution
<i>ent</i>	entrained
<i>exhaust</i>	exhaust
<i>i</i>	index representing the orientation of wall
<i>latent</i>	latent
<i>s</i>	supply air conditions
<i>sol</i>	solution
<i>o</i>	outdoor conditions
<i>w</i>	wall

# ILLUSTRATIONS

## Figure

1: Schematic showing the components of the studied system.....	5
2: Schematic of the space model showing the two separated zones. ....	6
3: Near wall boundary layer exchanging heat and mass with the dehumidifier and the room .....	8
4: Flow chart of the numerical methodology .....	17
5: (a) Schematic of dehumidifier assembly and (b) single membrane.....	19
6: Schematic of the experiment setup.....	20
7: Figures showing the thermocouples measurements of (a) boundary layer temperature and (b) solution temperature .....	22
8: Experimental validation of (a) the velocity field and (b) the temperature of the desiccant solution as function of the axial position .....	25
9: Design chart of LDMC-C/DV system at $T_{supply} = 18^{\circ}C$ , a $CaCl_2$ solution flow rate of $0.0277 \text{ kg/s}$ ( $4.0 \text{ kg/hr.m}^2$ of floor area) and concentration of 38 %, a load of $75 \text{ W/m}^2$ , a specific humidity ratio of 0.0138 kg of water vapor/kg of dry air .....	32
10: Design chart of LDMC-C/DV system at $T_{supply} = 20^{\circ}C$ , a $CaCl_2$ solution flow rate of $0.0277 \text{ kg/s}$ ( $4.0 \text{ kg/hr.m}^2$ of floor area) and concentration of 38 %, a load of $75 \text{ W/m}^2$ , a specific humidity ratio of 0.0138 kg of water vapor/kg of dry air .....	33
11: Design chart of LDMC-C/DV system at $T_{supply} = 22^{\circ}C$ , a $CaCl_2$ solution flow rate of $0.0277 \text{ kg/s}$ ( $4.0 \text{ kg/hr.m}^2$ of floor area) and concentration of 38 %, a load of $75 \text{ W/m}^2$ , a specific humidity ratio of 0.0138 kg of water vapor/kg of dry air .....	33
12: (a) The whole setup (b) Source Tank & recirculating pump (c) Humidifiers (d) Cooling Bath and Ice Cube and Packs and (e) Collector .....	43
13: (a) the top view of the dehumidifier showing the desiccant thermocouples and (b) side view of the wind tunnel showing boundary layer thermocouples and humidity sensors.....	44
14: Dehumidifier installed inside the chamber.....	44

15: Air supply grille and dehumidifiers.....	45
16: Computing the membrane weight.....	45

# TABLES

## Table

1: LDMC-C/DV - <i>PEC</i> design parameters and their operational ranges .....	31
--	----

## CHAPTER I

# COOLED LIQUID DESICCANT DEHUMIDIFICATION MEMBRANE CEILING & DISPLACEMENT VENTILATION

### **A. Introduction:**

Thermal comfort and indoor air quality are the most important characteristics of indoor environment (Atila et al. 2001). They are usually provided by conventional HVAC systems that often consume large amounts of energy (Hao et al. 2005). One of the HVAC systems that is known to be energy efficient is the combined chilled ceiling and displacement ventilation (CC/DV) system (Ghali et al., 2007; Mossolly et al., 2008; Keblawi et al., 2009; Ghaddar et al., 2010). The CC system removes heat sources directly by radiation and indirectly by convection enhancing thermal comfort with lower velocity in the occupied room (Novoselac et al. 2002, Keblawi et al. 2009). On the other hand, the DV system provides high indoor air quality by supplying fresh air with low air velocity directly to the occupied zone (Atila et al., 2002). However, the combination of the chilled ceiling and the displacement ventilation system has always been hindered by the risk of condensation of water on the cool ceiling (Niu et al., 2001) since frequent condensation leads to mold growth and potential IAQ problems (Mumma et al. , 2003).

In order to prevent condensation associated with CC/DV system, researchers have adopted two strategies. First, they limited the minimum temperature of the radiant cooling water to avoid condensation (Yin et al. 2009). However, this method will evidently decrease the heat reception capacity of the panel and limit its use to very low load situations. The other technique is to dehumidify the air outside the space to control

the supply air humidity such that the air leaving the space at the ceiling has lower dew point temperature than the chilled ceiling temperature (Keblawi et al., 2009; Mossolly et al., 2008; Zhang et al. 2003). Nevertheless, dehumidification of air outside the space is energy intensive with some drawbacks. It could be achieved either by cooling the air to a temperature below its dew point temperature to remove moisture, and then reheating it to the set design supply temperature (Abed-Salam et al., 2014) or by using solid or liquid desiccant dehumidification systems (Isetti et al., 1996; Bergero et al. 2000, Niu et al., 2001; Zhang et al., 2012; Abed-Salam et al., 2014; Itani et al. 2015). The first method will lead to a potential growth in the cooling coil while the second will risk the entrainment of the liquid desiccant increasing the consequent possibility of inhaling hazardous desiccants. To resolve the issue of dehumidification using the membrane without condensation or carry-over of desiccants, researchers have used the membrane inside the space to allow for effective radiant cooling by allowing lower chilled ceiling operating temperatures (Fauchoux et al. 2010; Eldeeb et al. 2013; Keniar et al. 2015). In this case, the air and the liquid desiccant streams are separated from each other by a membrane (hydrophilic water adsorbent material/hydrophobic water non-adsorbent material) allowing the water vapor and heat transport (Bergero et al. 2000; Huang et al., 2013). The energy implications and possible savings were studied by Muslmani et al. (2016) who developed a model to predict performance of a liquid desiccant membrane chilled ceiling combined with displacement ventilation system (LDMC-C/DV) at relatively low cooled ceiling temperature. They reported that decreasing the membrane liquid desiccant temperature resulted in significant decrease of the total cooling energy of



the system and a decrease of 49% in energy consumption when compared to the conventional CC/DV system.

Nevertheless, Muslmani et al. model (2016) had drawbacks. Their model assumed that the whole upper zone of the conditioned space is at uniform well-mixed conditions similar to the methods used for conventional CC/DV conditioned spaces. But, the presence of the permeable liquid desiccant ceiling that allows water vapor to transfer into the membrane may result in the formation of a ceiling adjacent flow zone that cannot be assumed to have the same conditions of the room upper zone. This zone, where the heat and water vapor transfer occurs needs to be studied thoroughly and incorporated to the space model to have accurate predictions of temperature and humidity adjacent to the ceiling where the risk of condensation is highest. Indeed, the use of membrane system does not provide the indoor humidity control; thus, when the DV supply conditions are very humid, the system risks condensation to occur on its housing (John Morphy et al., 2011). This is because the support and the frame of the housing is usually composed by a metal such as aluminum. The risk of condensation at the housing part of the ceiling is explained by the presence of two competitive phenomena: the extraction of the sensible heat losses by the chilled ceiling system and the extraction of the moisture by the liquid desiccant membrane system. If the extraction of heat phenomena overcomes the extraction of moisture, the risk of condensation might increase in situations when the air adjacent to the membrane surface is saturated. In addition, their model did not consider the limitation on the operational parameters of the membrane system in avoiding the risk of condensation at low ceiling temperature while providing thermal comfort in the occupied zone. Therefore, it is necessary to find the feasible operational conditions of the

LDMC-C/DV system similar to the approach adopted by Keblawi et al. (2009) for developing conventional CC/DV design charts. These charts permitted the user to read off directly from the charts the feasible operational parameters such as the supply conditions, chilled ceiling temperature, the ratio of CC sensible load removal to the total sensible load removed by the combined CC/DV system, and the displaced air parameter (the ratio of the total sensible load ratio to the supply air mass flow rate).

However, the design/sizing of the LDMC-C/DV system is not straightforward as the case of CC/DV system and needs to be investigated thoroughly. Clearly, the presence of permeable cooled membrane adds new operational parameters that need to be considered in the design of the system. Indeed, the membrane ceiling temperature will be affected by the uncontrolled humidity of room air influenced by the outdoor humidity. Besides, the inlet desiccant solution temperature as well as its mass flow rate will play an influential role on the ceiling membrane temperature.

Therefore, it is of great interest to address these shortcomings by: (i) developing an accurate but simplified model that is based on solving the heat and mass equations on the vicinity of the membrane at both air and solution desiccant sides and (ii) developing appropriate design charts permitting the prediction of the system feasible operational parameters for comfort and indoor air quality. The simplified model is validated by conducting a suitable experiment and comparing the measured and predicted outcomes. After integrating the validated model with the space model, the design charts are developed by performing several simulations that cover several operational parameters where the ceiling temperature is much lower than the conventional CC/DV system values reported in previous studies.

## B. System Description:

**Figure 1** shows a schematic of a space conditioned by a DV system combined with a ceiling membrane cooled by liquid desiccant solution. Liquid desiccant is flowing over the ceiling membrane exchanging heat and water vapor from the air flowing near the wall throughout the permeable membrane. In the presence of the DV system, the supply fresh cool air enters the room at the floor level and raises the warm air (by natural convection) to the exhaust grill placed at the ceiling level (Cho et al. 2005). Moreover, the internal load elements induce the formation of the stratification height at which the flow in the plumes becomes equal to the supply flow rate leading to the formation of two zones: occupied and contaminated zones separated at the stratification height (Novoselac et al. 2002, Ghali et al. 2007) as shown in **Figure 2**. The lower occupied zone is a thermally comfortable zone with an acceptable air quality while the upper unoccupied zone is a contaminated zone where neither thermal nor IAQ is a concern.

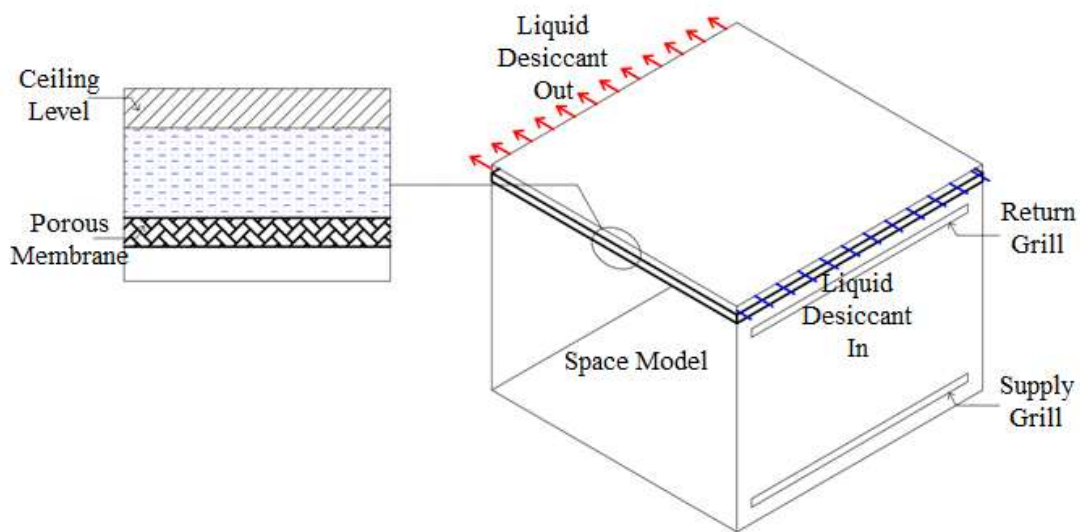


**Figure 1:** Schematic showing the components of the studied system

The thermal space model has been extensively studied in the literature (Mundt 1996; Novaselac et al. 2002, Keblawi et al. 2011) where the upper mixed zone is considered homogenous. However, the flow of the air over the permeable cooled ceiling creates a near wall boundary layer that exchanges heat and mass with the liquid desiccant solution which renders the assumption of the homogeneity of the upper zone invalid. In this study, in order to improve the predictions of air conditions adjacent to the ceiling membrane, the thermal space model will be modified such that the upper zone is divided into a mixing zone and an adjacent to membrane boundary layer region where air is entrained in until it leaves through the exhaust grill as will be described in the research methodology section.

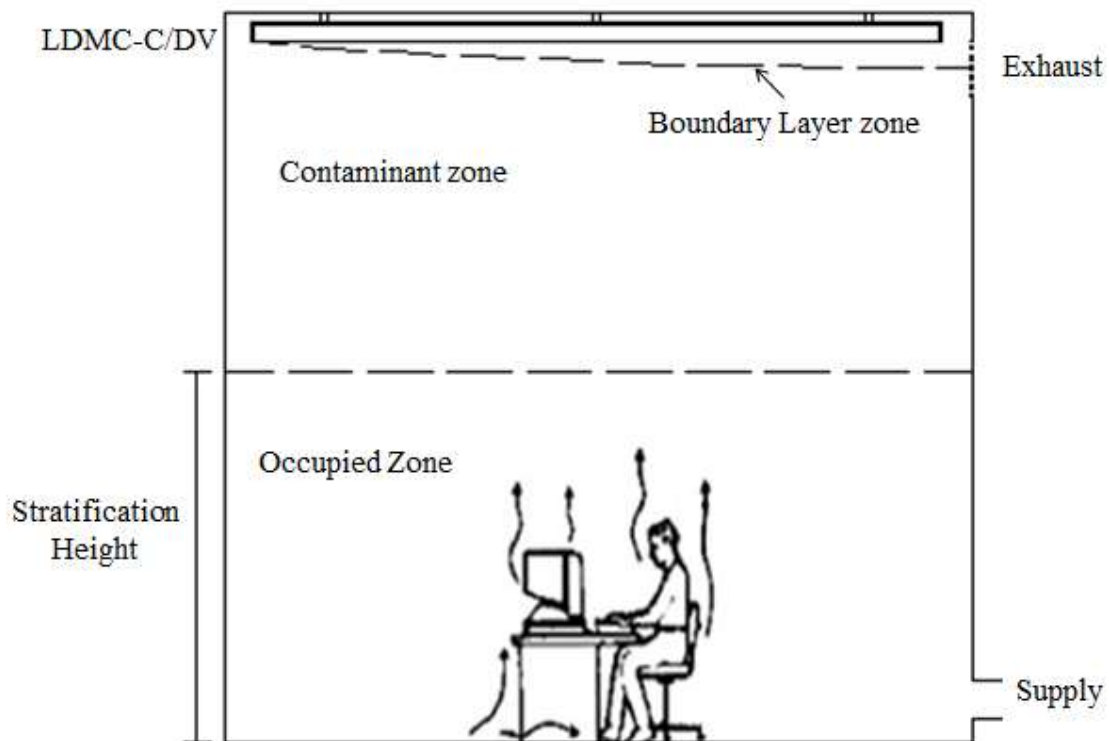


**Figure 2:** Schematic of the space model showing the two separated zones

## CHAPTER II

### DEVELOPMENT & INTEGRATION OF BL-DEHUMIDIFIER MODEL WITH SPACE MODEL SYSTEM

The research methodology begins by a mathematical model that investigates the heat and mass transfer through the permeable membrane between the liquid desiccant flow and the adjacent air layer. The air drawn by the exhaust grill forms a near wall boundary layer over the ceiling. In this boundary layer, the heat and water vapor transfers occur between the air and the solution desiccant throughout the permeable membrane. The boundary layer model is validated experimentally in a controlled environmental chamber.

Following the validation of the membrane boundary layer model, the model is then integrated with the space model of the LDMC-C/DV composed of the lower occupied zone and the upper contaminated well-mixed zone as shown in **Figure 2** (Muslmani et al., 2016). The integrated mathematical model of membrane system and the space model is then used to develop the system design charts. These charts for a given system load would indicate the feasible operational parameters when both thermal comfort and air quality are ensured in the occupied zone and when there is no risk of condensation on the cooled ceiling.

### A. Mathematical model of ceiling dehumidifier (air layer and liquid desiccant flow sides)

The heat and mass transfer occurs between the liquid desiccant flowing in the dehumidifier zone and the air flowing over the ceiling forming a near wall boundary layer as shown in **Figure 3**. The heat and mass conservation equations are formulated for the desiccant air side and the air layer side zones under the following assumptions:

- (i) one dimensional heat and mass variation,
- (ii) no energy or mass storage in the boundary layer zone or in the chilled ceiling panel where the liquid desiccant is flowing at steady state conditions (the ceiling temperature  $T_c$  is equal to the solution temperature  $T_{sol}$ ),
- (iii) the axial heat conduction and vapor diffusion are neglected,
- (iv) constant latent heat due to the small temperature range (Keniar et al., 2015),
- (v) the velocity, mass, and temperature boundary layer thicknesses of air are considered equal ( $Pr \approx Sc \approx 1$ ).

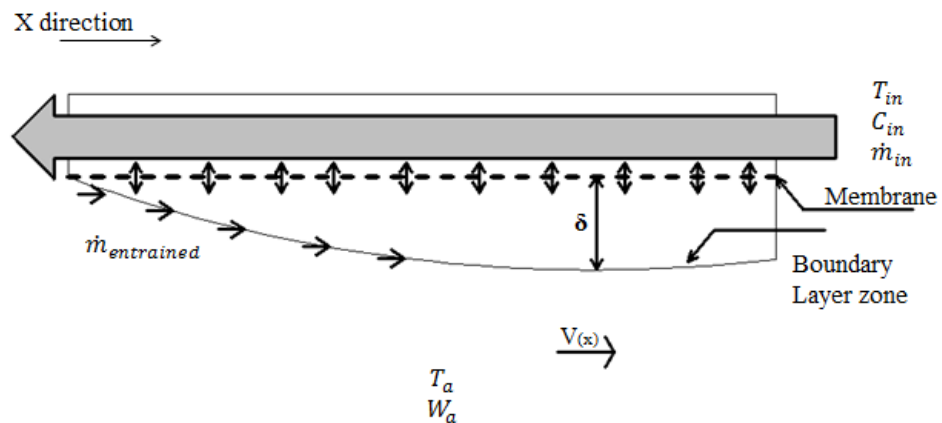


**Figure 3:** Near- wall boundary layer exchanging heat and mass with the dehumidifier and the room

## B. Liquid desiccant flow side

It is assumed that the air and the desiccant solution are flowing in opposite directions (counter-flow mode). In the dehumidifier zone, the liquid desiccant is entering at  $\dot{m}_{in}$ ,  $T_{in}$ ,  $C_{in}$  and absorbs heat and moisture throughout the membrane which is hydrophobic, permeable to water vapor but impermeable to liquid desiccant solution. On the other side, the air is drawn by the exhaust grill and some air is entrained along the boundary layer ( $\dot{m}_{entrained}$ ). In order to predict the variation of the desiccant temperature and the concentration, the moisture and energy conservation balances are solved. Considering the above-mentioned assumptions, the heat and moisture transfer equations developed for the desiccant side are respectively given by

$$-\dot{m}_{sol} \frac{d}{dx} (cp_{sol} T_{sol}) + U_c W_m (T_{BL} - T_{sol}) + \rho_a h_{fg} U_m W_m (w_{BL} - w_{sol}) = 0 \quad (1)$$

$$-\dot{m}_{sol} \frac{d}{dx} (C_{sol}) + \rho_a U_m W_m (w_{BL} - w_{sol}) = 0 \quad (2)$$

where  $\dot{m}_{sol}$ ,  $T_{sol}$ ,  $C_{sol}$ ,  $cp_{sol}$ ,  $w_{sol}$  are the solution mass flow rate, temperature, concentration, and humidity ratio respectively, while  $T_{BL}$ ,  $w_{BL}$  are the air temperature, and humidity ratio respectively,  $U_c$ ,  $U_m$ , and  $h_{fg}$  are the heat transfer coefficient, mass transfer coefficient, and the latent heat respectively.

In Eq. (1), the first term represents the net convective energy flow; the second term represents the sensible energy added to the solution due to the temperature difference between the boundary layer and the solution, while the last term accounts for the latent heat absorbed due to the moisture transfer between the air in the boundary layer and the solution. In Eq. (2), the first term represents the net convective moisture flow, while the second term accounts for the moisture transport between the air in the boundary layer and

the solution. Finally, the overall heat and mass transfer coefficients,  $U_c$  and  $U_m$  are given by [19]:

$$U_c = \left( \frac{1}{h_{ci}} + \frac{t}{k} + \frac{1}{h_{co}} \right)^{-1} \quad (2a)$$

$$U_m = \left( \frac{1}{h_{mo}} + \frac{t}{D_a} \right)^{-1} \quad (2b)$$

where  $h_{ci}$ ,  $h_{co}$  are the heat transfer coefficient at the inside and outside the dehumidifier,  $h_{mo}$  is the mass transfer coefficient outside the dehumidifier,  $k$  and  $D_a$  are the thermal conductivity and the diffusivity of water vapor in air, and  $t$  is the thickness of the membrane.

### C. Air boundary layer side

In order to solve for the heat and mass transfer inside the boundary layer, it is necessary to find the local boundary layer thickness which is a function of the velocity of air flowing over the ceiling induced by the presence of the exhaust at the wall near the ceiling level as shown in Figure 3. However, the velocity of air flowing over the ceiling is not constant and reaches its maximum at the exhaust level (Awbi et al. 2003).

Researchers have used different tools to determine velocity gradients. Some have investigated the velocity field numerically using detailed computational fluid dynamic software (Lin et al. 2005, Yan et al. 2009 ) while others reported the velocity field experimentally using particle image velocimetry (Kang et al., 2009). Both techniques proved that the presence of exhaust in a confined room resulted in a velocity variation as function of the distance from the studied point to the exhaust position. Awbi et al.(Awbi



et al. 2003) reported that the velocity distribution is a function of the distance  $x$  to the exhaust grill, the height of the exhaust grill, and the exhaust velocity as follows:

$$V_{\infty,x}(x) = V_{\infty} \times \frac{1}{1 + 4\sqrt{((L_p - x) / h)^3}} \quad (3)$$

where  $h$  is the height of the exhaust,  $L_p$  is the length of the panel, and  $V_{\infty}$  is the outlet velocity deduced by dividing the supply flow rate to the exhaust area.

The momentum conservation applied on a differential element of length  $dx$  in the boundary layer zone states that the momentum variation is equal to the forces on this element (Schlichting et al. 2017) and is given by

$$-\frac{\partial}{\partial x} \int_0^{\delta} \rho V_x^2(x) dy + \dot{m}_{entrained}(x) V_{\infty,x}(x) = \mu \left. \frac{\partial V_x(x)}{\partial y} \right|_{y=0} \quad (4)$$

where the entrained mass flow rate  $\dot{m}_{entrained}$  into the near ceiling boundary layer, can be deduced by applying the conservation of mass on a differential element of length  $dx$  in the boundary layer zone and is given by

$$\dot{m}_{entrained}(x) = \int_0^{\delta} \frac{d(\rho u)}{dx} w dx dy \quad (5)$$

Assuming a linear profile of the velocity inside the boundary layer zone ( $V_x(x) = \frac{V_{\infty,x}(x)y}{\delta(x)}$ ) that satisfies the no-slip condition at the ceiling, and substituting Eq.

(4) into Eq. (5), the differential equation of the boundary layer thickness at each location  $x$  is given by the following equation:

$$-\delta(x) \frac{V_{\infty,x}(x)}{6} \frac{dV_{\infty,x}(x)}{dx} + \frac{V_{\infty,x}^2(x)}{6} \frac{d\delta(x)}{dx} + \frac{\mu}{\rho} \frac{V_{\infty,x}(x)}{\delta(x)} = 0 \quad (6)$$

where  $\delta(x)$  is the local thickness of the boundary layer zone,  $\mu$  and  $\rho_a$  are the dynamic viscosity and density of air respectively. The differential equation of the boundary layer thickness is subjected to Dirichlet boundary conditions at the onset as follows:

$$V_{\infty,x}(0) = 0 \quad \text{and} \quad \delta(0) = 0 \quad (7a)$$

However, at the exhaust level, the gradient of the boundary layer thickness is null while the velocity is constant as following:

$$V_{\infty,x}(L_p) = V_\infty \quad \text{and} \quad \frac{d\delta(L_p)}{dx} = 0 \quad (7b)$$

Applying the energy and water vapor conservation at the air side results in equations (8) and (9) respectively as follows:

$$\begin{aligned} -\dot{m}_{BL}(x) \frac{d}{dx} (c p_a T_{BL}(x)) + U_c W_m (T_{sol}(x) - T_{BL}(x)) \\ + \rho_a h_{fg} U_m W_m (w_{sol}(x) - w_{BL}(x)) + \frac{\dot{m}_{entrained}(x) c p_a T_a(x)}{dx} = 0 \end{aligned} \quad (8)$$

$$-\dot{m}_{BL}(x) \frac{d}{dx} (w_{BL}(x)) + \rho_a U_m W_m (w_{sol}(x) - w_{BL}(x)) + \frac{\dot{m}_{entrained}(x) w_a(x)}{dx} = 0 \quad (9)$$

where  $T_a$  and  $w_a$  are the entrained mass flow rate temperature and humidity ratio respectively,  $\dot{m}_{BL}$  is the air mass flow rate entering a differential element of the air boundary layer.

The first term of Eq. (8) represents the net convective energy flow in the boundary layer; the second term represents the sensible energy added to the solution due to the temperature difference between the boundary layer and the solution, the third term accounts for the latent heat absorbed due to the moisture transport between the air in the boundary layer and the solution, while the last term represents the convective energy flow of the entrained air from the room. In Eq. (9), the first term represents the net convective

moisture flow in the boundary layer, the second term accounts for the moisture transport between the air in the boundary layer and the solution, while the last term represents the convective moisture flow of the entrained air from the room.

#### D. Integration with space model system

The boundary layer model will be integrated with the two-zone space model to solve for the temperature and humidity conditions in the occupied lower zone, the upper well mixed zone, and the boundary layer zone.

Equations (1) to (9) assume lumped conditions of  $T_a$  and  $w_a$  for the upper zone and estimates the spatial temperature and humidity of air inside the boundary layer zone as well as the temperature and concentration of the liquid desiccant inside the chilled ceiling. When integrated with the space model (see **Figure 2**),  $T_a$  and  $w_a$  represent the temperature and the water vapor of the contaminated upper zone from which air is entrained. Therefore, the energy and mass balance of the upper unoccupied zone are given by the following equations respectively:

$$0 = \dot{m}_S C_{p,a} T_{a,o} - \int_0^{Lp} \dot{m}_{entrained(x)} C_{p,a} T_a dx - m_{exhaust} C_{p,a} T_a + Q_{light} + \sum (h_i A_{w,i} (T_w - T_a)) \quad (10 a)$$

$$0 = \dot{m}_S \omega_{a,o} - \int_0^{Lp} \dot{m}_{entrained(x)} \omega_a dx - m_{exhaust} \omega_a \quad (10 b)$$

The first, second and third terms of the right hand side of the energy balance Eq. (10 a) represent respectively the rate of energy transferred (i) from the occupied zone to the contaminated upper zone due to buoyancy; (ii) from the contaminant zone to the boundary layer zone by the entrained mass flow rate over the width of the ceiling

membrane; (iii) from the contaminant zone to the outdoor due to fan captivation though the exhaust grill. The fourth term represents the energy added due to heat produced by lights; the last term represents the convective heat transfer between the indoor air space and the zone's wall. The mass balance Eq. 10(b) accounts for the incoming air from the occupied zone, entrained air into the boundary layer and the exhaust air.

The lower occupied zone exchanges heat with the room walls, and gains heat from the electrical equipment. People occupying the room are transferring sensible and latent heat to the occupied zone. On the other hand, the supply air entering from DV system exchanges heat and water vapor with the lower zone. Therefore, the steady state mass and energy conservation for the lower occupied zone at  $T_{a,o}$  and  $w_{a,o}$  are given by the following equations respectively:

$$0 = \dot{m}_S C_{p,a} (T_S - T_{a,o}) + \sum (h_i A_{w,i} (T_W - T_{a,o})) + q_{elec} + q_{people} \quad (11 a)$$

$$0 = \dot{m}_S (w_S - w_{a,o}) + \frac{q_{Latent}}{h_{fg}} \quad (11 b)$$

The first term of the right hand side of Eq. (11 a) represents the net convective heat transfer between the supply air and the occupied zone. The second term represents the convection heat transfer between the indoor air space and the room's wall. Finally, the last two terms represent the amount of sensible heat generated by electric equipment and occupants respectively. The first term of the right hand side of Eq. (11 b) represents the net convective moisture transfer between the supply air and the occupied zone. The last term accounts for the rate of moisture generation (kg/s) by occupants.

In order to calculate the stratification height which is a measure of air quality in the occupied zone, the upward air flow rate due to the plumes is determined. Assuming that

the walls are at uniform inner surface temperature, the mass flow rate of plumes generated from wall can be modeled using Jaluria's model (1980) equation:

$$M_w = 0.00287 \times \rho \times \Delta T_w^{0.25} \times z^{\frac{3}{4}} \times W \quad (12)$$

where

$$\Delta T_w = T_w - T_a \quad (13)$$

The plume generated from a point heat source with a heat transfer rate  $q$  can be determined by solving the below equations (14 a), (14 b) and (14 c) for a zone with internal air having a temperature gradient (Mundt 1995) and are expressed as follows:

$$Q_{plume} = 0.00238 \times q^{3/4} \left( \frac{dT_a}{dz} \right)^{-5/8} \times B_1 \quad (14 a)$$

$$B_1 = 0.004 + 0.039A_1 + 0.38A_1^2 - 0.062A_1^3 \quad (14 b)$$

$$A_1 = 2.86 \times Z \left( \frac{dT_a}{dz} \right)^{3/8} q^{-1/4} \quad (14 c)$$

Thus the equation used to determine the stratification height is given by

$$\dot{m}_s = \rho_a Q_s = N \rho_a Q_{plume} + \rho_a \sum_{k=1}^n Q_{u,k} \quad (15)$$

Where  $Q_s$  is the supply air volumetric flow rate,  $\dot{m}_s$  is the air supply flow rate,  $N$  is the number of point sources inside the room, and  $n$  is the number of walls.

## E. Numerical Methodology

Mathematical models for the space and permeable liquid desiccant ceiling are discretized and integrated to predict the condition of the air in the boundary layer

(temperature and humidity) as well as the temperature and concentration of the desiccant system. The numerical methods and the integration of DV space with LDMC-C models is shown in **Figure 4**. The inputs for the integrated system are represented by the outdoor weather conditions, supply air conditions of flow rate, temperature and relative humidity, internal loads, envelope properties and space, and liquid desiccant ceiling setup geometry and physical dimensions as well as the liquid desiccant properties, inlet temperature, concentration and flow rate.

The coupled mass and energy equations are discretized into algebraic equations using the finite volume method. The axial  $x$ -direction is divided into 100 nodes and grid independency is tested at each simulation. The temperature profile in the space in addition to the walls and ceiling temperatures are first assumed. Then, the DV space thermal model solves the energy balance equations, taking into account the thermal plumes from internal heat sources as well as wall plumes, to obtain the temperature and humidity in lower and upper zones. The air conditions in the upper zones are used as input to the ceiling-adjacent boundary layer zone and the liquid desiccant flow model to solve for temperature and humidity distribution at the ceiling as well as the liquid desiccant exit temperature and concentration. The ceiling temperature is then updated to the average value of the permeable membrane temperature. The previous steps are repeated until convergence in ceiling temperature, where the relative error does not exceed  $10^{-6}$ . Once convergence is reached, the temperature distribution in the space is determined as well as the thermal comfort and air quality conditions of the vertical temperature gradient, the Predicted Mean Value (PMV), and the stratification height  $H_S$ .

In addition, sensible and latent heat losses removed by each sub system (DV and LDMC- ) are computed for the converged case.

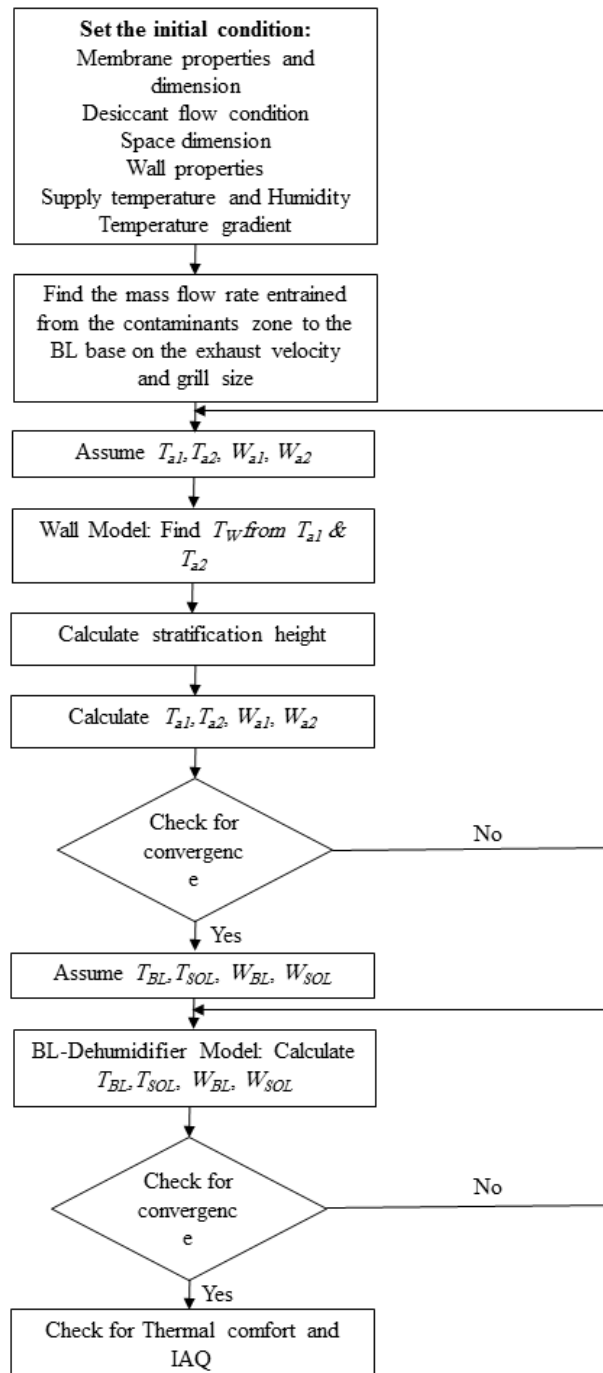


Fig.4: Flow chart of the numerical methodology

## CHAPTER II

### EXPERIMENTAL SETUP & MODEL VALIDATION

The validity of the dehumidifier boundary layer mathematical model is ensured by conducting experiments in which the rate of moisture removal by the desiccant solution, and the temperature distribution in the desiccant flow and compared with the values predicted by the developed mathematical model of the membrane system. Calcium Chloride ( $\text{CaCl}_2$ ) is selected as the desiccant solution, due to its moisture absorption capacity and low cost.

#### **A. The membrane ceiling panel**

The selection of the membrane's material is very critical; it should be permeable to water vapor but impermeable to liquid water. Furthermore, the membrane should be characterized by small resistance to heat and moisture transfer (Awbi et al. 2003). Polypropylene membranes from Sterlitech (Kent, WA, USA) were acquired (Sterlitech Corporation). Each membrane sheet is  $200 \times 200$  mm area and a thickness of  $110 \mu\text{m}$ . An analytical balance (Radwag AS 220, R2) was used to weigh the membrane sheet with a standard deviation of  $0.1$  mg and the bulk density was deduced (Choi et al., 2015). The porosity was determined to be 80% (Ma et al. 2005). The thermal conductivity of this type of the membrane is  $0.0608$  W/m·K (Georgieva et al. 2010).

Five membrane sheets were adhered to each other using black construction Silicone, the only material that does not harm the membranes and holds them tightly with no leakage. The assembled membrane is joined to the dehumidifier frame using epoxy resin



along its perimeter. The dehumidifier's frame is made from Plexiglas of 1 m long, 20 cm wide and 1cm height. In addition, baffles were installed to the duct for two reasons: the first is to guide the solution and cover the whole membrane's area to absorb water vapor, and the second is to fortify the membranes' stability preventing their sag as shown in **Figure 5**.

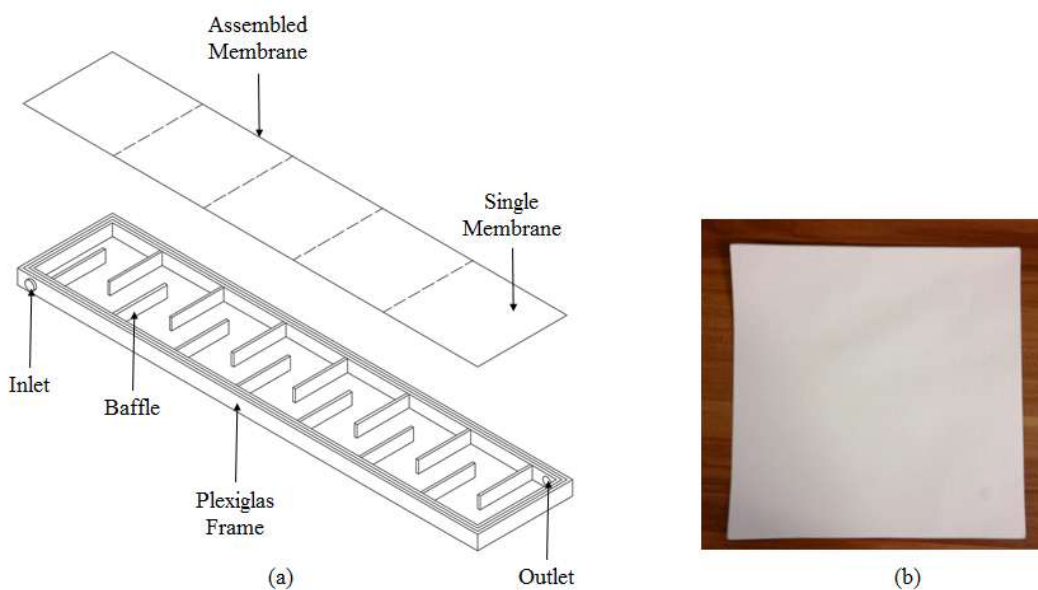


**Figure 5:** (a) Schematic of dehumidifier assembly and (b) Single membrane photo

## B. The experimental setup

A schematic of the open circuit experimental set up presenting the experiment components is shown in **Figure 6**. The Plexiglas duct of 1 m length is placed in a closed duct of 0.8 m × 0.8 m cross sectional area installed in a climatic chamber as shown in the figure where the exhaust fan is drawing the air in the opposite direction of the desiccant flow through an exhaust grill of 17 cm height. Four humidifiers is placed at the supply grill of 25×25 cm cross sectional area to humidify the supply air entering the

experimental duct. A cooling bath is used to cool the desiccant solution to the desired inlet temperature. Since the desiccant flow is an open cycle. The desiccant solution is stored in a reservoir that would insure at least four hours of continuous flow. A circulating pump is utilized to direct the desiccant from the stored tank to the membrane system and final to a collector reservoir. The flow is regulated by a globe valve.

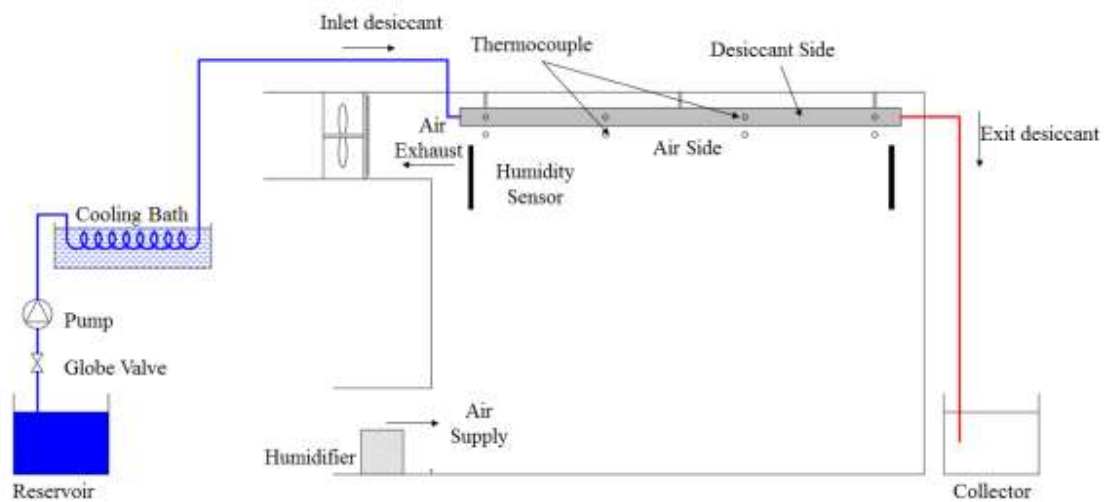


Figure 6: Schematic of the experiment setup

### C. Experimental measurements and protocol

The top of the dehumidifier panel is pierced at four different locations distributed equally in order to install four thermocouples. The thermocouples are used to record the desiccant temperature change in its axial direction. In addition, another two similar thermocouples are installed close to the panel in the air side to monitor the change in the air temperature at point A and point B (near the exhaust) as shown in Figure. 6. The eight thermocouples used are of K-type bought from OMEGA with 0.01 °C accuracy. Furthermore, two relative humidity sensors (OMEGA HX94A series 2.5% accuracy) are

mounted at the beginning and end of the duct (points A and B) to check the relative humidity change in adjacent air flow due to the presence of the liquid desiccant above the membrane. **Figure. 6** shows the location of all used sensors. The velocity distribution along the air side external to the boundary layer was measured using a hot wire anemometer device (OMEGA HHF2005HW model). It is characterized by an accuracy of  $\pm 10\%$  of full scale velocity measurement. The hot wire anemometer was placed at four locations distributed along the duct on the air side.

A solution was prepared from Calcium Chloride and water and was stored in the source tank. The liquid desiccant is pumped away from the reservoir to the cooling bath using a recirculating pump with a mass flow of  $0.1 \text{ kg/hr}$  ( $\pm 10^{-3} \text{ kg/hr}$ ) measured by using a reservoir and a stop watch and controlled by the globe valve. The desiccant's pipe is immersed in the cooling bath to cool it down to the desired inlet temperature of  $16.4 \text{ }^\circ\text{C}$  before entering the dehumidifier duct. The desiccant solution removes moisture and heat from the air layer adjacent to the membrane and is collected finally in another reservoir. The experiment is held in a room temperature  $T_a = 22.1 \text{ }^\circ\text{C}$  and a relative humidity  $RH = 70.7\%$ . The fan is rotating to bring  $81.6 \text{ l/s}$  of air from the duct leading to an exhaust velocity of  $0.6 \text{ m/s}$ . The inlet solution concentration of the desiccant solution was  $38 \%$  and its inlet temperature was  $16.4^\circ\text{C}$ .

After turning on the suction fan and regulating the globe valve, the sensors are turned on to take the temperature and the humidity readings, and the experimental set up was left to operate for 3 hours. The measurements were saved after observing the temperature and relative humidity stabilized where the fluctuations become less than  $3 \%$  of the instantaneous value relative to the average measured values over one hour of the

temperature and humidity ratio. The measurements taken for the temperature at the boundary layer and the desiccant zones are shown in Figure 7 (a) and 7 (b) respectively.

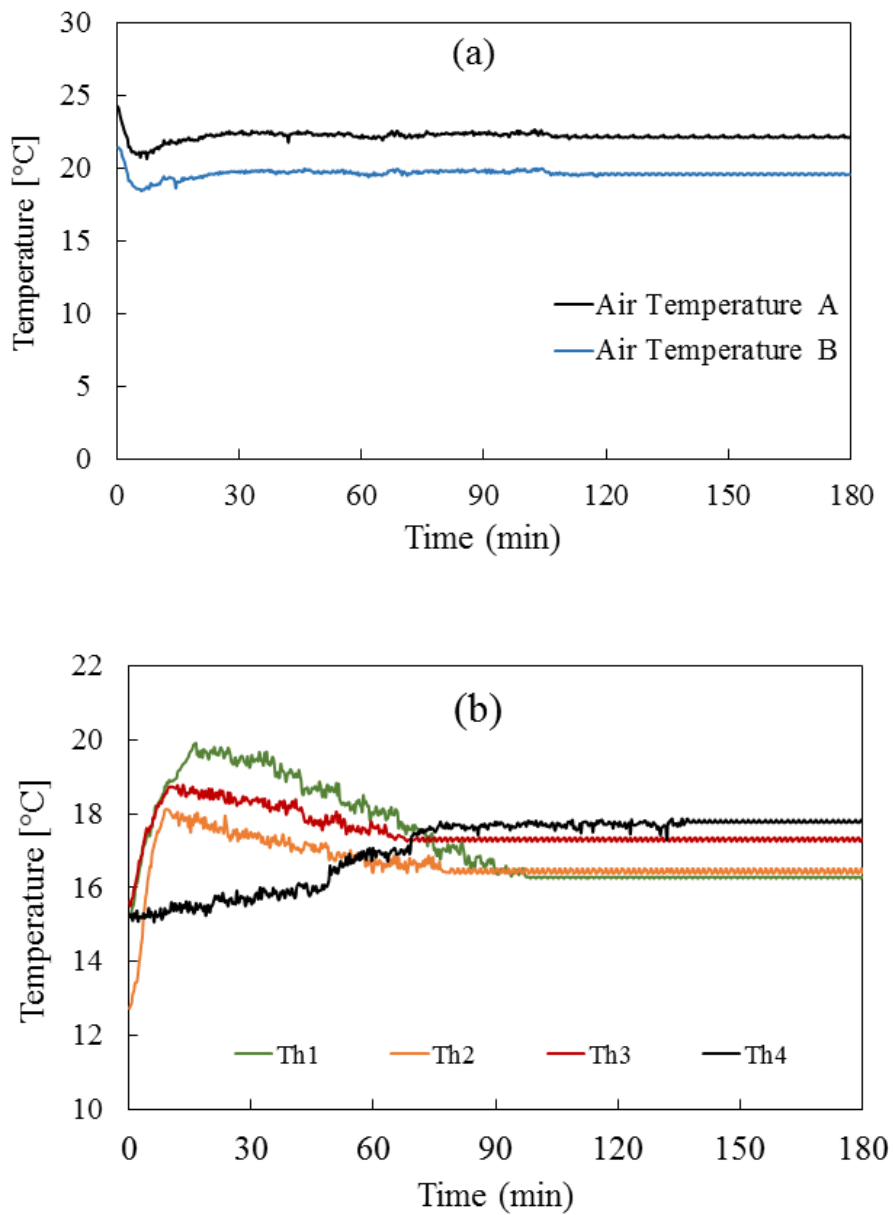


**Figure 7:** Figures showing the thermocouples measurements of (a) boundary layer temperature and (b) solution temperature

#### **D. Experimental Validation of the mathematical model**

The mathematical model developed for the boundary layer side associated with the motion of air on the plate over which the desiccant solution flows was simulated for the geometric and physical parameters of the experiment while using the experimentally measured inlet desiccant and air conditions.

Since the boundary layer model simulation results depends on the air velocity distribution in  $x$ , the measured velocity was compared to the predicted velocity distribution outside the boundary layer close to the ceiling membrane panel. **Figure 8(a)** shows that the velocity distribution provided by Awbi et al. (2003) and used in the mathematical model agrees with the experimental findings with an average relative error of 10%. It was shown that the velocity reaches its maximum at the exhaust where withdrawal occurs while the velocity gradient is maximum at the air inlet side. **Figure 8(b)** shows the temperature distribution of the desiccant side. Since the air is exchanging sensible and latent heat to the desiccant solution through the membrane, the calcium chloride solution temperature increased from its inlet to its outlet flow sides by 1.53 °C. The experimentally measured desiccant temperature distribution was also compared with the model. Good agreement is shown between the experiment and the mathematical model with a maximum relative error of 4%.

In order to insure the validity of the mathematical model, the results given by the two relative humidity sensors mounted adjacent to the membrane at points A and B are compared with the predicted relative humidity by the developed mathematical model. Both the model prediction and the experiment show that the relative humidity is approximately unchanged and it is about 70 %. The main reason is that the decrease in

relative humidity caused by the decrease of the humidity ratio is compensated by the decrease in the air temperature of the boundary layer. In addition, the measured drop in air temperature was 2.54 °C from the outer main stream value of 22.13 °C at Point **A** and the exhaust value close to the membrane panel at point **B**. The model prediction of change in boundary layer temperature was 2.7 °C which is slightly higher than the measured value since it is experimentally affected by the main stream air temperature at location **B**.

Furthermore, the outlet solution concentration is also measured and validated with the mathematical model. It is shown that the solution concentration varies slightly from 38% to 37%. This finding agreed well with the finding of Keniar et al. (2015).

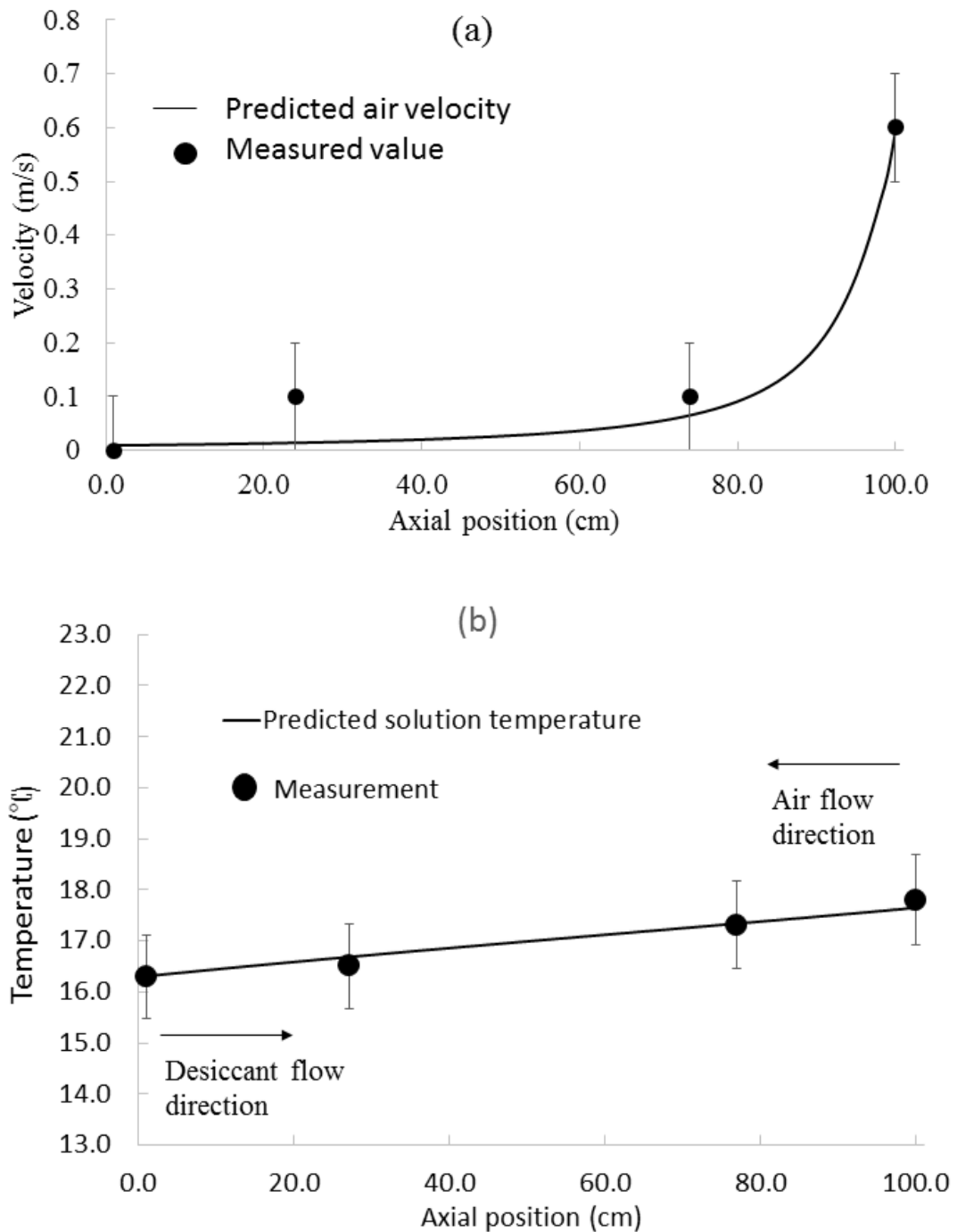


**Figure 8:** Experimental validation of (a) the velocity field and (b) the temperature of the boundary layer and desiccant solution as function of the axial position

## CHAPTER IV

### GENERATION OF DESIGN CHARTS FOR THE APPROPRIATE OPERATIONAL CONDITIONS OF LDMC-C/DV SYSTEM

For any cooling system, the ultimate goal is to provide efficiently a good level of thermal comfort for the occupant in the context of their task and their environment condition. For the current LDMC-C/DV system, one additional objective would be ensuring that no condensation takes place at the cooled ceiling. For this reason, more design parameters need to be determined as compared with the conventional CC/DV system and would result in introducing changes in the previously developed CC/DV charts of Keblawi et al. (2009).

The conventional CC/DV design chart represented two important design parameters as function of temperatures of the DV supply and the chilled ceiling (Ghaddar et al. (2008); Keblawi et al. (2009); Mirzaie et al. 2015). These parameters were i) the ratio  $R$  of sensible load removed by the CC to the total sensible load removal by both subsystems; ii) the DV supply flow rate parameter  $P$  which is the ratio of the total sensible load in kW to the DV supply mass flow rate ( $\dot{m}_s$ ) in kg/s and is given by

$$P = \frac{Q_{space} (KW)}{\dot{m}_s (kg / s)} (kJ / kg)$$

(12)

where  $Q_{space}$  represents the sensible thermal and  $\dot{m}_s$  is the DV supply mass flow rate of air in kg/s. The proposed design charts for the LDMC-C/DV will use similar parameters. However and due to the latent load removal by the ceiling, the split of the load will be



represented by the parameter  $R$  which is the ratio of heat removal (sensible + latent) from the ceiling to the total load of both the ceiling ( $Q_{chilled\ ceiling}$ ) and the DV ( $Q_{DV}$ ) subsystem and is defined as follows:

$$R = \frac{Q_{Chilled\ ceiling}}{Q_{DV} + Q_{Chilled\ ceiling}} \quad (13)$$

The integrated model of LDMC-C/DV can be used to predict load removal by each of the membrane system and the DV system, the temperatures and humidity of the lower, upper, and boundary layer zones and the stratification height for given space load. This permits the identification of  $P$  and  $R$  for a feasible combination of operational parameters to meet desired thermal comfort, air quality, and no condensation requirements for the following operational parameters of the LDMC-C/DV:

- Inlet temperature of the desiccant solution into the membrane system ( $T_{solution}$  in °C)
- Desiccant solution flow rate  $\dot{m}_{sol}$  in l/s
- Desiccant solution inlet concentration
- DV supply temperature ( $T_{supply}$  in °C)
- DV supply humidity ratio (kg H<sub>2</sub>O/kg of dry air)

Since the number of operational parameters of the hybrid system are too many, it is not possible to have them all represented in a single chart. Each design chart will be generated for a given load at fixed DV supply temperature and humidity ratio. Furthermore, each chart will show the ratio  $R$  as a function of inlet solution temperature  $T_{solution}$  for different  $P$ . The DV supply flow rate and temperature and the liquid desiccant flow rate and temperature are to be selected to remove the room peak thermal load such that thermal comfort is provided in the lower occupied zone. The criteria that ensure that

thermal comfort, good air quality are attained and the risk of condensation is eliminated are:

- The temperature gradient does not exceed 2.5 °C/m. This condition is required so that the human is not subject to large gradients in temperature between head and feet that cause thermal discomfort (ASHRAE 2009). In addition, the Predicted Mean Vote in the occupied zone “PMV” is to be ensured within  $\pm 0.5$  for thermal comfort (Fanger, 1982; Fang et al. 2004). The PMV condition is included since the temperature gradient condition does not account for possible high humidity in the occupied zone that may cause discomfort.
- The stratification height inside the room is greater than 1.1 m. This condition is required so that fresh air clean zone is above a seated human head to ensure good air quality in the occupant breathing zone (ASHRAE 2009).
- The relative humidity of the air boundary layer zone adjacent to the ceiling is less than 95%. There is an increased risk of condensation if the liquid desiccant is unable to remove enough moisture and the ceiling temperature reaches a value below the dew point of the boundary layer air. In addition, condensation could occur at the supporting structure or mesh that is typically made of light metal.

With the above given criteria, five different zones of operating conditions for the LDMC-C/DV system can be identified and will be shown in the design chart(Figure 9,10 & 11 ) as follows:

- Zone I: Thermal comfort is achieved and no condensation occurs on the ceiling (Desired and feasible operational range of the LDMC-DV system)
- Zone II: Thermal comfort is achieved but condensation can occur on the ceiling

- Zone III: No thermal comfort can be attained and no condensation occurs on the ceiling
- Zone IV: No thermal comfort can be attained and condensation can occur on the ceiling
- Zone V: Poor Air quality zone due to low DV flow rate resulting in stratification height lower than 1.1 m.

## CHAPTER V

### CASE STUDY

A case study is adopted for the generation of the design charts for a typical office space with dimensions  $5\text{m} \times 5\text{m} \times 3\text{m}$ , located in Beirut Lebanon. A maximum number of 6 occupants are considered inside the room. Each one generates  $1.38 \times 10^{-5}$  kg/s of water vapor, 70 W of sensible heat and uses a computer producing a heat power of 65 W. The room is equipped with a light having a power of  $15 \text{ W/m}^2$  which makes the total load inside the room about 1860 W (= **75 W/m<sup>2</sup>** of floor area). The ambient design temperature of the outside air is assumed at  $T_{\infty}=34 \text{ }^{\circ}\text{C}$  while the humidity ratio is 0.01382 kg of water/kg of dry air reflecting a typical moderate humid climate summer day

In order to generate the design charts representing the appropriate operational conditions of LDMC-C/DV, 1200 simulations have been performed using the developed integrated space and membrane system model. The input to the simulations are the inlet solution temperature, its concentration and its mass flow rate, the inlet DV supply air temperature, its humidity ratio and its mass flow rate, and the load. The outputs of the simulations are the temperature and the humidity ratio at the occupied and unoccupied zones, as well as the amount of heat removed from the chilled ceiling and from the DV system.

The range of the design parameters including the supply air solution temperature are summarized in Table 1. The DV supply air humidity ratio is 0.01382 kg of water/kg which is equal to outdoor humidity since no dehumidification is applied to the supply air. The inlet mass flow rate of the desiccant solution has a very narrow range dictated by the condition that the temperature difference between the solution at inlet and exit from the

room should be small. Hence, a constant inlet desiccant mass flow rate of 0.0277 kg/s (4.0 kg/hr·m<sup>2</sup> of floor area) is justified and is used in the model. The inlet concentration of the desiccant solution is assumed 0.38 in mass basis of CaCl<sub>2</sub> and this presents the value recommended in literature for good affinity to water vapor without the possibility of salt crystallization at small temperature ( $\geq 13^{\circ}\text{C}$ ) [19, 21,42,43]. The main output that will be shown in the developed design charts is the amount of heat removed by chilled permeable ceiling obtained from the parameter  $R$  for a selected DV flow rate parameter  $P$  in the feasible zone of operation.

<b>Design parameter</b>	<b>Operational range</b>
Solution temperature ( $T_{solution}$ in $^{\circ}\text{C}$ )	13 to 22
Solution flow rate (kg/s)	0.0277
Solution concentration in mass basis of CaCl <sub>2</sub>	0.38
DV supply temperature ( $T_s$ in $^{\circ}\text{C}$ )	18 to 22
Panel dimension (m)	4m × 4m
$P$ (kJ/kg)	3 - 15
Predicted Mean Vote, PMV	Acceptable Comfort Range from -0.5 to +0.5
Stratification height (m)	$\geq 1.1$

Table 1. LDMC-C/DV -PEC design parameters and their operational ranges

### A. Description of the LDMC-C/DV design charts with an example

For the fixed space load of  $75\text{W/m}^2$ , three LDMC-C/DV design charts are generated for DV supply air temperatures of 18, 20 and 22 °C as shown in Figure 9, 10, 11, respectively where the load split parameter  $R$  is plotted vs the inlet desiccant solution temperature at different flow rate parameter  $P$  while identifying the five zones defined in chapter IV.

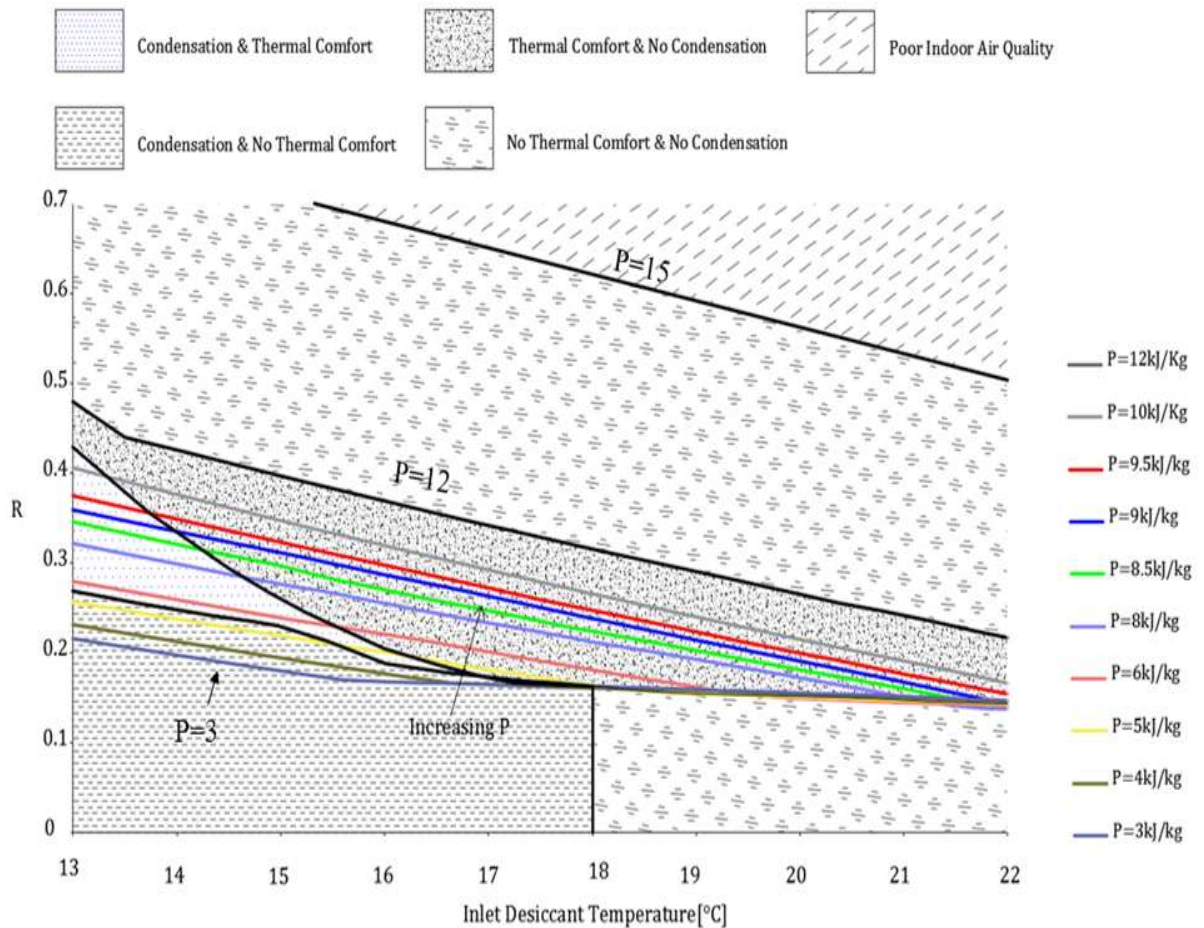


**Figure 9** Design chart of LDMC-C/DV system at  $T_{supply} = 18^\circ\text{C}$ , a  $\text{CaCl}_2$  solution flow rate of  $0.0277\text{ kg/s}$  ( $4.0\text{ kg/hr.m}^2$  of floor area) and concentration of 38 %, a load of  $75\text{ W/m}^2$ , a specific humidity ratio of  $0.0138\text{ kg}$  of water vapor/kg of dry air

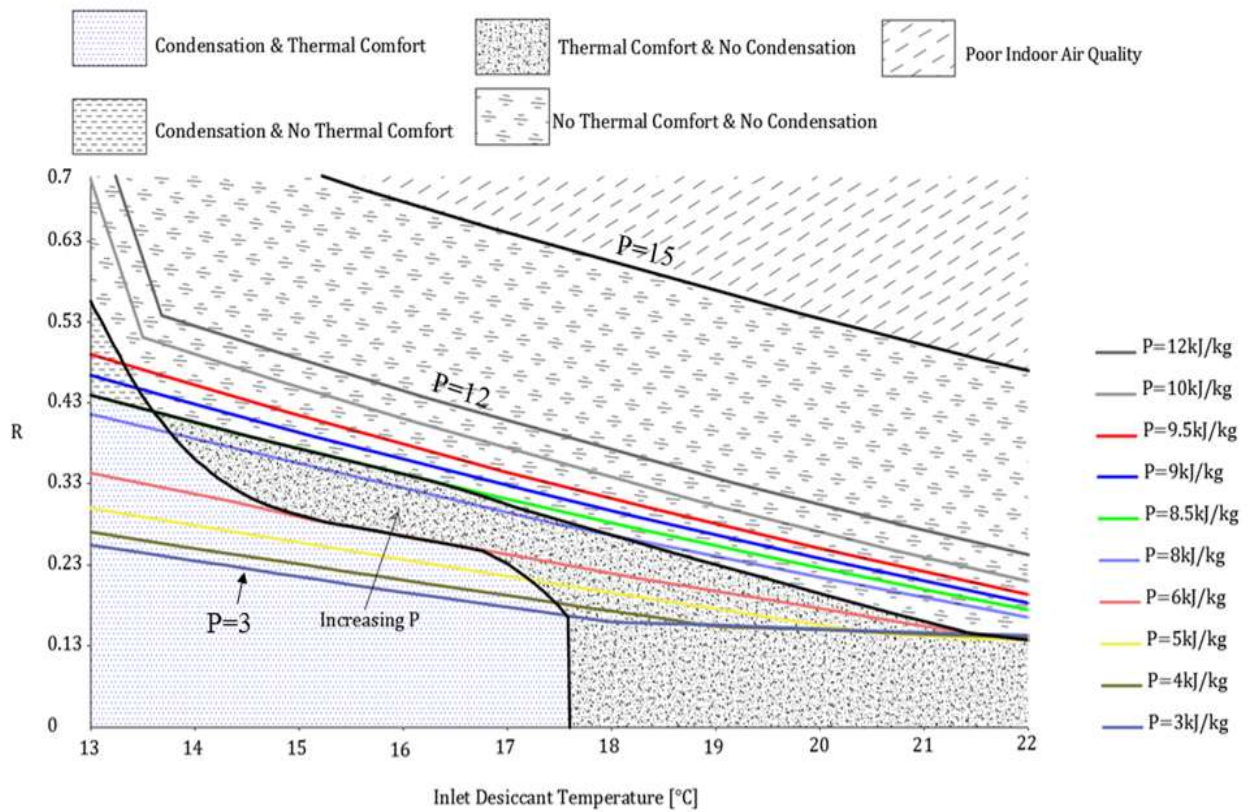


**Fig. 10** Design chart of LDMC-C/DV system at  $T_{supply} = 20^{\circ}\text{C}$ , a  $\text{CaCl}_2$  solution flow rate of  $0.0277 \text{ kg/s}$  ( $4.0 \text{ kg/hr.m}^2$  of floor area) and concentration of 38 %, a load of  $75 \text{ W/m}^2$ , a specific humidity ratio of  $0.0138 \text{ kg}$  of water vapor/kg of dry air

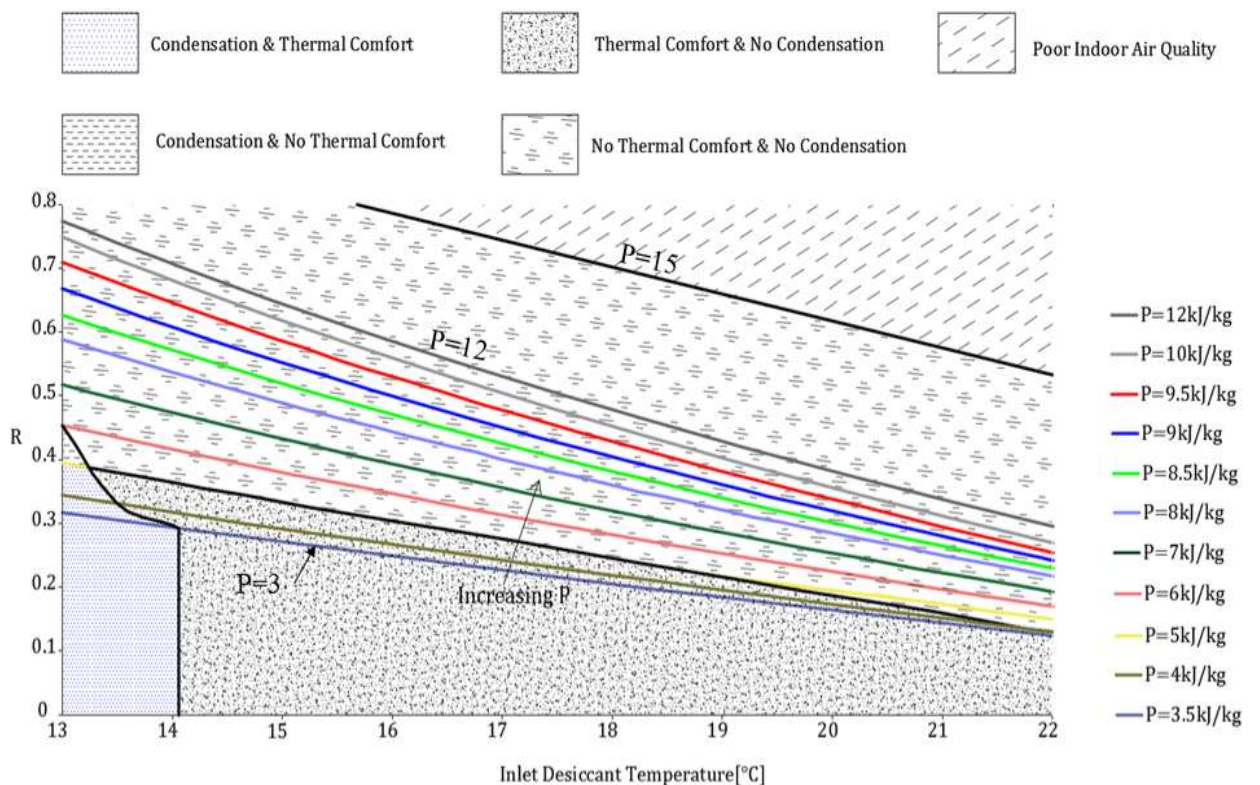


**Fig. 11** Design chart of LDMC-C/DV system at  $T_{supply} = 22^{\circ}\text{C}$ , a  $\text{CaCl}_2$  solution flow rate  $0.0277 \text{ kg/s}$  ( $4.0 \text{ kg/hr.m}^2$  of floor area) and concentration of 38 %, a load of  $75 \text{ W/m}^2$ , a specific humidity ratio of  $0.0138 \text{ kg}$  of water vapor/kg of dry air



**Figure 9** shows the variation of  $R$  values at different  $P$  for different inlet solution temperature at a fixed supply temperature of 18 °C. It is clear that at an inlet solution temperature smaller than 13.5 °C, condensation occurs at all  $P$ -lines. When the solution temperature increases, condensation is prevented and the thermal comfort attainment depends on the value of  $P$  reflecting the inlet supply flow rate at DV system. When  $P$  is relatively low (3 to 5 kJ/kg), the DV mass flow rate is large leading to more fresh air entering the chamber at a low supply temperature of 18°C and hence results in thermal discomfort. For large value of  $P$ , the DV mass flow rate is small leading to poor air quality because there is insufficient fresh air entering the space and stratification height would be less than 1.1 m. Consequently, the zone of thermal comfort and no condensation is delimited by the other four zones considering the limits on CaCl<sub>2</sub> solution temperature to prevent condensation as well as the limits on  $P$  to ensure enough supply flow rate to maintain good air quality and ensure comfort. Another observation is that at high value of  $P$ , the decrease in the DV mass flow rate is compensated by the chilled ceiling cooling which results in a larger value of  $R$ . At higher DV supply temperature 20°C, the design chart is shown in **Figure 10** and it is clear that the thermal comfort zone has shifted downward when compared to the design chart of Figure 9 at supply temperature of 18 °C. In other words, when the supply air temperature increases, the thermal comfort necessitates higher inlet air supply flow rate to remove the load. This higher inlet flow rate is reflected by decreasing the parameter  $P$  leading to the downward shift of the thermal comfort zone. The higher supply DV air temperature resulted in the reduction of the condensation zone and in having lower  $P$  values in the comfort zone.



This is evidently related to the increase of the air temperature in the room preventing the risk of condensation. The same observations were shown in **Figure 11** for higher supply temperature of 22 °C.

According to the design charts of Figure 9-11, two main observations could be drawn: (i) the condensation area is decreasing and (ii) the thermal comfort area is shifted down as the supply air temperature is increasing. The first observation is essentially related to the fact that any increase in supply air temperature increases the air temperature inside the space which limits the heat transfer with the ceiling. Raising the temperature of the ceiling above the dew point temperature of the adjacent air prevents the occurrence of possible condensation. While the second observation is associated with the need to increasing the DV supply temperature resulted in increasing the DV air flow to meet the space load. This increase in supply air flow rate is reflected by a decrease in  $P$ -value; thus shifting down the thermal comfort zone.

For a given supply air and desiccant temperature conditions, the design charts of Figure 9-11 can be used to find the feasible operational conditions and the part of the load removed by the chilled ceiling ( $R$ -value) compared to the total load. It can be seen for example that if a DV supply air temperature of 20 °C and a calcium chloride solution temperature of 15 °C, then using the chart in Fig. 10 one can obtain a feasible value of  $P = 8$  kJ/kg and its corresponding heat removal ratio by the chilled ceiling  $R = 0.34$  is obtained. Focusing on the comfort zone, different values can be used of  $P$  ranging from 3 to 9 kJ/kg and values of  $R$  ranging from 0.3 to 0.5 for different CaCl<sub>2</sub> inlet solution temperature. Thus the charts would present a convenient method for sizing the LDMC-C/DV system.

## **B. Conclusion**

In this paper, a mathematical model of the boundary layer side associated with the motion of air on the ceiling over which the desiccant solution flows in a LDMC-C/DV system is developed. The model is based on solving the heat and mass transfer through the membrane that is exposed to the boundary layer air in one side and to the solution desiccant in other side. The model is validated by conducting an appropriate experiment where temperature and humidity measurements show good agreement with a relative error of 4%. It is shown that the solution desiccant temperature increases by absorbing the heat and the moisture from the air at the boundary layer side. The boundary layer air temperature and humidity ratio is decreasing consequently. When the model is coupled to the space model, different design charts are developed at different supply air temperatures. These design charts are used to find the operational parameters that influence the meeting of the LDMC-C/DV objectives of comfort, air quality and no condensation on the ceiling for a fixed load. Furthermore, they specify the amount of heat removed by the chilled ceiling over the total load as function of the inlet solution desiccant temperature and the supply air flow rate. It is shown that when the supply air temperature increases, condensation zone decreases, thermal comfort zone is shifted down towards the large supply flow rate.

## BIBLIOGRAPHY

- Novoselac A, Srebric J. A critical review on the performance and design of combined cooled ceiling and displacement ventilation systems. *Energy and Buildings* 2002;34: 497–509. doi: 10.1016/s0378-7788(01)00134-7.
- Hao X, Zhang G, Chen Y, Zou S, Moschandreas DJ. A combined system of chilled ceiling, displacement ventilation and desiccant dehumidification. *Building and Environment* 2007;42: 3298–308. doi: 10.1016/j.buildenv.2006.08.020.
- Ghali K, Ghaddar N, Ayoub M. Chilled ceiling and displacement ventilation system for energy savings: A case study. *International Journal of Energy Research* 2007;31: 743–59. doi: 10.1002/er.1266.
- Mossolly M, Ghali K, Ghaddar N. Optimal control strategy for a multi-zone air conditioning system using a genetic algorithm. *Energy* 2009;34: 58–66. doi: 10.1016/j.energy.2008.10.001.
- Keblawi A, Ghaddar N, Ghali K, Jensen L. Chilled ceiling displacement ventilation design charts correlations to employ in optimized system operation for feasible load ranges. *Energy and Buildings* 2009; 41: 1155–64. doi: 10.1016/j.enbuild.2009.05.009.
- Ghaddar N, Ghali K, Saadeh R. Optimized selection and operation of the combined chilled ceiling system and displacement ventilation. *International Journal of Energy Research* 2010;34: 1328–40. doi: 10.1002/er.1677.
- Novoselac, A., Burley, B.J., Srebric, J. Development of new and validation of existing convection correlations for rooms with displacement ventilation systems. *Energy and Buildings* 2006; 38(3): 163-173

- Niu J, Zhang L, Zuo H. Energy savings potential of chilled-ceiling combined with desiccant cooling in hot and humid climates. *Energy and Buildings* 2002;34: 487–95. doi: 10.1016/s0378-7788(01)00132-3.
- Mumma S.A. Chilled Ceiling condensation control. *ASHRAE IAQ Applications*, 2003, p. 22–3.
- Yin Y, Wang R, Zhai X, Ishugah T. Experimental investigation on the heat transfer performance and water condensation phenomenon of radiant cooling panels. *Building and Environment* 2014; 71: 15–23. doi: 10.1016/j.buildenv.2013.09.016.
- Zhang L, Niu J. Indoor humidity behaviors associated with decoupled cooling in hot and humid climates. *Building and Environment* 2003; 38: 99–107. doi: 10.1016/s0360-1323(02)00018-5.
- Abdel-Salam AH, Ge G, Simonson CJ. Thermo-economic performance of a solar membrane liquid desiccant air conditioning system. *Solar Energy* 2014;102: 56–73. doi: 10.1016/j.solener.2013.12.036.
- Isetti C, Nannei E, Magrini A. On the application of a membrane air—liquid contactor for air dehumidification. *Energy and Buildings* 1997;25: 185–93. doi: 10.1016/s0378-7788(96)00993-0.
- Bergero S, Chiari A. Experimental and theoretical analysis of air humidification/dehumidification processes using hydrophobic capillary contactors. *Applied Thermal Engineering* 2001;21: 1119–35. doi: 10.1016/s1359-4311(00)00107-1.
- Zhang LZ, Huang SM, Pei LX. Conjugate heat and mass transfer in a cross-flow hollow fiber membrane contactor for liquid desiccant air dehumidification. *International journal of heat and mass transfer* 2012; 55:8061-72.

- Itani M, Ghali K, Ghaddar N. Increasing energy efficiency of displacement ventilation integrated with an evaporative-cooled ceiling for operation in hot humid climate. *Energy and Buildings* 2015;105: 26–36. doi: 10.1016/j.enbuild.2015.07.055.
- Fauchoux M, Bansal M, Talukdar P, Simonson CJ, Torvi D. Testing and modelling of a novel ceiling panel for maintaining space relative humidity by moisture transfer. *International Journal of Heat and Mass Transfer* 2010;53: 3961–8. doi: 10.1016/j.ijheatmasstransfer.2010.05.015.
- Eldeeb R, Fauchoux M, Simonson CJ. Applicability of a heat and moisture transfer panel (HAMP) for maintaining space relative humidity in an office building using TRNSYS. *Energy and Buildings* 2013;66: 338–45. doi: 10.1016/j.enbuild.2013.07.021.
- Keniar K, Ghali K, Ghaddar N. Study of solar regenerated membrane desiccant system to control humidity and decrease energy consumption in office spaces. *Applied Energy* 2015;138: 121–32. doi: 10.1016/j.apenergy.2014.10.071.
- Huang S-M, Yang M, Yang X. Performance analysis of a quasi-counter flow parallel-plate membrane contactor used for liquid desiccant air dehumidification. *Applied Thermal Engineering* 2014;63: 323–32. doi: 10.1016/j.applthermaleng.2013.11.027.
- Muslmani M, Ghaddar N, Ghali K. Performance of combined displacement ventilation and cooled ceiling liquid desiccant membrane system in Beirut climate. *Journal of Building Performance Simulation* 2016;9: 648–62. doi: 10.1080/19401493.2016.1185153.
- Morphy J. Understanding chilled beam systems . *Engineers Newsletter* 2011.38(4), 1-12
- Cho S, Im P, Haberl JS. Literature review of displacement ventilation. *Energy Systems Laboratory, Texas A&M University*; 2005.

Mundt E. The performance of displacement ventilation systems: Experimental and theoretical studies, 1996.

Keblawi A, Ghaddar N, Ghali K. Model-based optimal supervisory control of chilled ceiling displacement ventilation system. *Energy and Buildings* 2011;43: 1359–70. doi: 10.1016/j.enbuild.2011.01.021.

Awbi HB. *Ventilation of buildings*. Taylor & Francis; 2003.

Lin Z, Chow TT, Fong KF, Wang Q, Li Y. Comparison of performances of displacement and mixing ventilations. Part I: thermal comfort, *International journal of refrigeration* 2005; 28:276-87.

Yan W, Zhang Y, Sun Y, Li D. Experimental and CFD study of unsteady airborne pollutant transport within an aircraft cabin mock-up. *Building and Environment* 2009; 44:34-43.

Kang JH, Lee SJ. Investigation on the flow characteristics inside an automotive HVAC system with varying ventilation mode. *Journal of visualization* 2009; 12: 375-82.

Schlichting H, Gersten K, Krause E, Oertel H. *Boundary-layer theory*. Berlin: Springer; 2017.

Jaluria Y. *Natural convection: heat and mass transfer*. Elkins Park (Pa.): Franklin; 1994.

Bettahalli NS, Lefers R, Fedoroff N, Leiknes T, Nunes SP. Triple-bore hollow fiber membrane contactor for liquid desiccant based air dehumidification. *Journal of Membrane Science* 2016; 514: 135–42. doi: 10.1016/j.memsci.2016.04.059.

Sterlitech Corporation. Sterlitech. <https://www.sterlitech.com/> (accessed June 19, 2016).

Choi J, Yang BJ, Bae GN, Jung JH. Herbal extract incorporated nanofiber fabricated by an electrospinning technique and its application to antimicrobial air filtration. *ACS applied materials & interfaces* 2015;7:25313-20.

Ma Z, Kotaki M, Yong T, He W, Ramakrishna S. Surface engineering of electrospun polyethylene terephthalate (PET) nanofibers towards development of a new material for blood vessel engineering. *Biomaterials* 2005; 26:2527-36.

Georgieva S, Godjevargova T, Mita DG, Diano N, Menale C, Nicolucci C, Carratelli CR, Mita L, Golovinsky E. Non-isothermal bioremediation of waters polluted by phenol and some of its derivatives by laccase covalently immobilized on polypropylene membranes. *Journal of Molecular Catalysis B: Enzymatic* 2010;66: 210-8.

Ghaddar N, Ghali K, Saadeh R, Keblawi A. Design charts for combined chilled ceiling displacement ventilation system. *ASHRAE Transactions* 2008; 114:574-87.

Mirzai S, Ghaddar N, Ghali K, Keblawi A. Design charts for sizing CC/DV system aided with personalized evaporative cooler to the desired thermal comfort. *Energy and Buildings* 2015; 86:203-13.

ASHRAE Handbook -Fundamentals. 2009. American Society of Heating Refrigerating and Air-Conditioning Engineers. Chapter 9. Atlanta, USA.

Fang L, Wyon DP, Clausen G, Fanger PO. Impact of indoor air temperature and humidity in an office on perceived air quality, SBS symptoms and performance. *Indoor Air* 2004;14: 74–81. doi: 10.1111/j.1600-0668.2004.00276.x.

Fanger PO. Thermal comfort: analysis and applications in environmental engineering. Malabar, FL: Krieger; 1982.

Sahlot M, Riffat SB. Desiccant cooling systems: a review. *International Journal of Low-Carbon Technologies* 2016. doi: 10.1093/ijlct/ctv032.

Mei L, Dai Y. A technical review on use of liquid-desiccant dehumidification for air-conditioning application. *Renewable and Sustainable Energy Reviews* 2008; 12: 662–89. doi: 10.1016/j.rser.2006.10.006.



## Appendix

### EXPERIMENT PICTURE

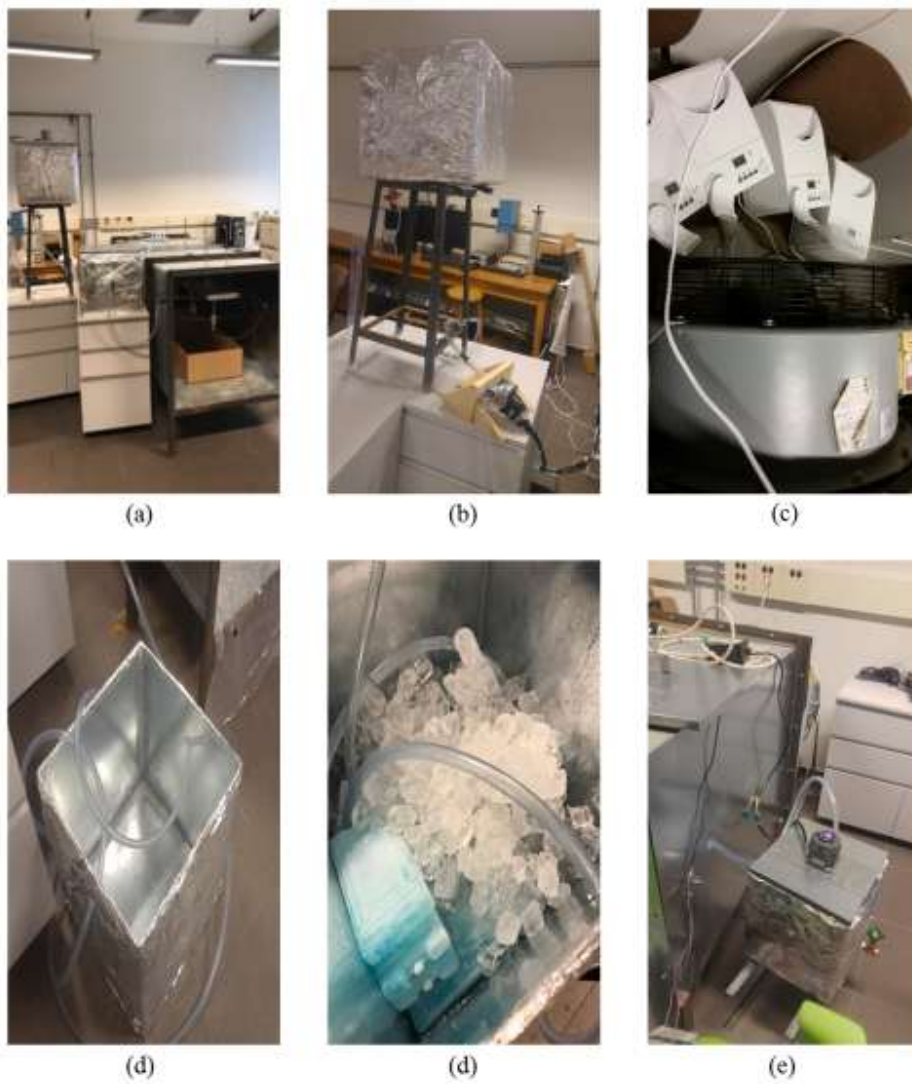


**Figure 12(a,b,c,d,e):** (a) The whole setup (b) Source Tank & recirculating pump (c) Humidifiers (d) Cooling Bath and Ice Cube and Packs and (e) Collector

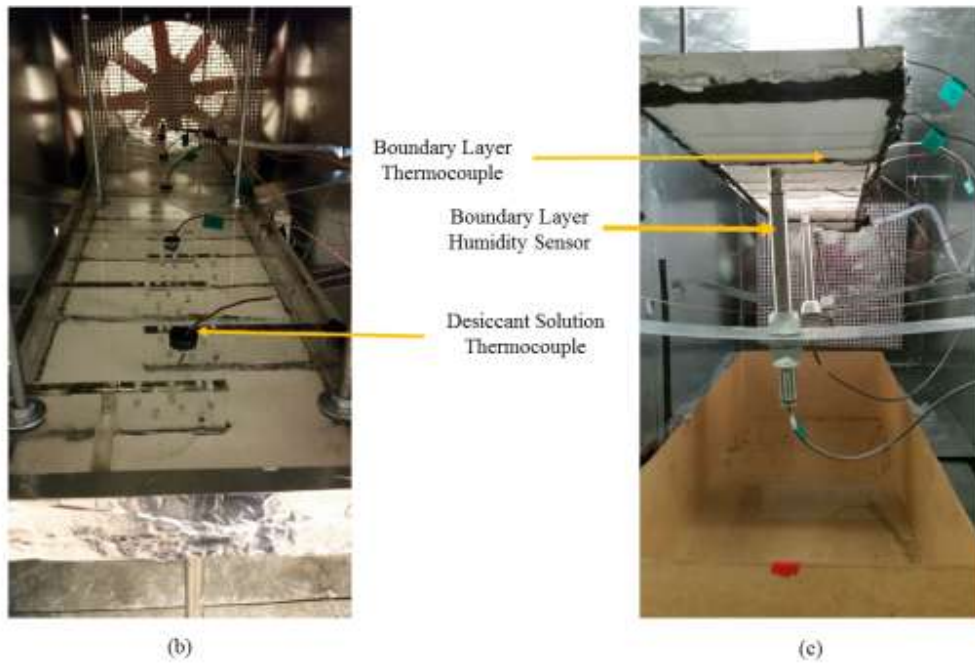


**Figure 13 (a,b):** (a) the top view of the dehumidifier showing the desiccant thermocouples and (b) side view of the wind tunnel showing boundary layer thermocouples and humidity sensors



**Figure 14:** Dehumidifier installed inside the chamber



Figure 15: Air supply grille and humidifiers



Figure 16: Computing the membrane weight